Title: Improved fluorescence assays to measure the defects associated with F508del-CFTR allow identification of new active compounds

Running Title: Improved fluorescence assays for monitoring CFTR

Emily Langron[1], Michela I. Simone[2], Clémence M.S. Delalande[3], Jean-Louis Reymond[3], David L. Selwood[4] and Paola Vergani[1]

[1] Research Department of Neuroscience, Physiology and Pharmacology

University College London

Gower Street

London WC1E 6BT

UK

[2] Discipline of Chemistry, School of Environmental and Life Sciences,

Priority Research Centre for Chemical Biology and Clinical Pharmacology

The University of Newcastle

University Drive

Callaghan, NSW 2308, Australia.

[3] Department of Chemistry and Biochemistry

University of Bern

Freiestrasse 3, BERN 3012

Switzerland

[4] Wolfson Institute for Biomedical Research

University College London

The Cruciform Building

Gower Street

London WC1E 6BT

UK

Correspondence to: emily.langron.12@ucl.ac.uk; p.vergani@ucl.ac.uk

Abstract

BACKGROUND AND PURPOSE

Cystic fibrosis (CF) is a debilitating disease caused by mutations in the cystic fibrosis transmembrane conductance regulator (*CFTR*) gene, which codes for a Cl^-/HCO_3^- channel. F508del, the most common CF-associated mutation, causes both gating and biogenesis defects in the CFTR protein. This paper describes the optimisation of two fluorescence assays, capable of measuring CFTR function and cellular localisation, and their use in a pilot drug screen.

EXPERIMENTAL APPROACH

HEK293 cells expressing YFP-F508del-CFTR, in which halide sensitive YFP is tagged to the N-terminal of CFTR, were used to screen a small library of compounds based on the VX-770 scaffold. Cells expressing F508del-CFTR-pHTomato, in which a pH sensor is tagged to the fourth extracellular loop of CFTR, were used to measure CFTR plasma membrane exposure following chronic treatment with the novel potentiators.

KEY RESULTS

Active compounds with efficacy ~50% of VX-770, micromolar potency, and structurally distinct from VX-770 were identified in the screen. The F508del-CFTR-pHTomato assay suggests that the hit compound MS131A, unlike VX-770, does not decrease membrane exposure of F508del-CFTR.

CONCLUSIONS AND IMPLICATIONS

Negative influence on F508del-CFTR biogenesis/stability by most known potentiators requires membrane exposure to be monitored early during development of drugs targeting CFTR. Combined use of the two fluorescence assays described here provides a useful tool for the identification of improved potentiators and correctors. The assays could also prove useful for basic scientific investigation on F508del-CFTR, and other CF-causing mutations.

TARGETS
Ion channels
CFTR

LIGANDS
Forskolin
VX-770, Ivacaftor
VX-809, Lumacaftor

These Tables of Links list key protein targets and ligands in this article that are hyperlinked* to corresponding entries in http://www.guidetopharmacology.org, the common portal for data from the IUPHAR/BPS Guide to PHARMACOLOGY (Southan et al., 2016), and are permanently archived in The Concise Guide to PHARMACOLOGY 2015/16 (Alexander et al., 2015).

Abbreviations

CF   Cystic Fibrosis

CFTR   Cystic Fibrosis Transmembrane conductance Regulator

$\varDelta F_{M}$ change in fluorescence reporting on membrane-localised CFTR-pHTomato

ΔF_{IN} change in fluorescence reporting on CFTR-pHTomato in biosynthetic vesicles

EC_{50} half-maximal effective concentration

eGFP   enhanced Green Fluorescent Protein

F/F_{max} normalised YFP fluorescence

$F_{pHTomato}$ weighted average fluorescence obtained during pHTomato assay

GFP   Green Fluorescent Protein

MES   2-(N-morpholino)ethanesulfonic acid

n_H	Hill coefficient
P_o	open probability
RFU	Relative Fluorescence Units
SSMD	strictly standardised mean difference
τ_{ib}	interburst duration
τ_b	burst duration
YFP	yellow fluorescent protein
WT	wild type

Introduction

Cystic fibrosis (CF) is the most common life-shortening hereditary disease in the Caucasian population, affecting approximately 10,800 patients in the UK alone (UK CF Registry annual report 2015). The disease is caused by mutations in the cystic fibrosis transmembrane conductance regulator (*CFTR*) gene, which codes for the CFTR anion channel (Riordan et al., 1989). To date, over 2,000 mutations have been identified (www.genet.sickkids.on.ca; www.cftr2.org). Approximately 90% of patients, however, carry at least one copy of F508del, the most common CF-causing mutation, which results in both a biogenesis and a gating defect in the CFTR protein (Cheng et al., 1990; Dalemans et al., 1991). F508del prevents maturation to complex-glycosylated, plasma membrane-located CFTR (Cheng et al., 1990). A global misfolding of the protein causes retention of F508del-CFTR at the endoplasmic reticulum, from where it is targeted for proteasomal degradation (Ward et al., 1995). Any F508del-CFTR which escapes degradation and reaches the plasma membrane has a short half-life (< 4 h; Lukacs et al., 1993), due to increased degradation and reduced recycling (Okiyoneda et al., 2010). F508del-CFTR membrane exposure can be improved in the lab using low temperature incubation, allowing the study of ion channel function (Denning et al., 1992). Using this technique, the open probability (P_o) of F508del-CFTR was measured as being ~15-fold smaller than that of wild type (WT)-CFTR (Miki et al., 2010), indicating a severe gating defect.

In 2012, VX-770 (Ivacaftor, Vertex Pharmaceuticals) became the first drug targeting the CFTR protein, approved for treatment of CF. Acting on the root cause, VX-770 has demonstrated a clear positive impact in the clinic (Ramsey et al., 2011; Davies et al., 2013). However, it is only effective for CF caused by G551D and a number of other, less common, gating mutations (Van Goor et al., 2009; Yu et al., 2012). The G551D mutation causes severe gating defects, but does not affect folding or plasma membrane exposure (Gregory et al., 1991; Bompadre et al., 2007). Consistent with the pleiotropy of the F508del mutation, VX-770 alone was not effective on patients homozygous for F508del (Flume et al., 2012). Treatment of F508del-CF will likely require a combination of a corrector compound, such as VX-809 (Lumacaftor, Vertex Pharmaceuticals), to promote F508del-CFTR membrane localisation, together with a potentiator, to increase P_o (Rowe and Verkman, 2013). An example of one such combination therapy, Orkambi (VX-770+VX-809, Vertex Pharmaceuticals), was recently approved for the treatment of F508del homozygous patients. A Phase III study revealed a mean absolute improvement in lung function (measured by forced expiratory volume in one second), of $2.6 - 4\%$ (Wainwright et al., 2015). Compared to *in vitro* results using acute VX-770 treatment alongside chronic VX-809 (conductance up to 30% of WT-CFTR; Van Goor et al., 2011), clinical efficacy was low.

It has since been shown that chronic VX-770 treatment decreases F508del-CFTR membrane exposure, regardless of the method of rescue (Cholon et al., 2014; Veit et al., 2014). The same was true of all potentiators that were tested, except one (Veit et al., 2014). The negative effect of chronic VX-770 on F508del-CFTR biogenesis and stability possibly contributed to the relatively disappointing Orkambi clinical trial results (but see Matthes et al., 2016).

This paper describes two fluorescence assays, capable of measuring the defects associated with F508del-CFTR: inefficient gating and defective biogenesis, resulting in low steady-state levels of CFTR protein at the plasma membrane. Yellow fluorescent protein (YFP)-CFTR, in which halide sensitive YFP (Galietta et al., 2001a) is tagged to the N-terminal of CFTR, provides a sensitive readout of CFTR function. CFTR-pHTomato, with a pH sensor tagged to the fourth extracellular loop of CFTR, can quantify membrane and internal CFTR, independently of each other, and independently of function.

YFP-F508del-CFTR was used to screen a pilot library of compounds with some structural similarity to VX-770. The hits from this screen were tested for long-term F508del-CFTR destabilisation effects, using the F508del-CFTR-pHTomato assay.

Methods

YFP-CFTR

GFP-CFTR, in which enhanced GFP (eGFP) is tagged to the N-terminal of CFTR via a 23 amino acid linker, was kindly provided by Bruce Stanton (Geisel School of Medicine, NH), in pcDNA3.1. To obtain YFP-CFTR, eight mutations (F46L, L64F, S65G, V68L, S72A, H148Q, I152L and T203Y) were introduced in eGFP-CFTR, using site-directed mutagenesis (Quikchange protocol, Stratagene).

CFTR-pHTomato

CFTR-pHTomato is expressed from the pIRES2-eGFP plasmid, which contains an internal ribosome entry site (IRES). This plasmid directs transcription of a single mRNA, containing coding sequences for both CFTR-pHTomato and eGFP, and translation of the two separate proteins. WT-CFTR in pIRES2-eGFP (pIRES-eGFP-CFTR) was a gift from David Gadsby (Rockefeller University, NY). pHTomato in the pRham plasmid was provided by Dr Li (Peking University, China) and Prof. Richard Tsien (NYU School of Medicine, NY), while pcDNA3.1-CFTR was a gift from Luis Galietta (Istituto Gaslini, Genova, Italy). pHTomato was inserted at a position, following Asp901, known not to interfere with cellular processing and function (Howard et al., 1995; Schultz et al., 1997). Using a primer overlap-extension strategy *AgeI* and *BmtI* sites were first introduced within extracellular loop 4 in pcDNA3.1-CFTR. A fragment including the coding sequence for pHTomato, flanked by the two restriction sites, was obtained by PCR using the pRham-pHTomato plasmid as template. Following restriction digest and ligation to obtain pcDNA3.1-CFTR-pHTomato, the pHTomato insertion was subcloned into the pIRES2-eGFP-CFTR plasmid, using the *SalI* and *BspEI* restrictions sites, present in WT-CFTR.

Screening library and compound syntheses

The UCL Chemibank (a resource of diverse, mostly drug-like compounds) was searched for compounds with similarity to VX-770. A set of compounds sharing the quinolone scaffold of VX-770 were identified (patent WO2015189560A1). This set also

included dissimilar intermediates which were also screened to identify MS131A and MS134A. Similarity was calculated as Tanimoto coefficients of ECFP 4 fingerprints using Pipeline Pilot.

http://pubs.acs.org/doi/abs/10.1021/ci100050t

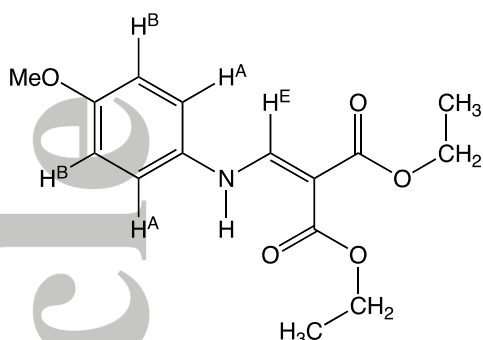**MS131A,** diethyl 2-(((3-(difluoromethoxy)phenyl)amino)methylene)malonate
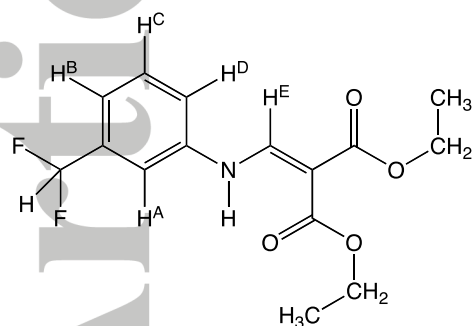
3-(Difluoromethoxy)aniline (0.51 g, 3.21 mmol) was stirred with diethyl ethoxymethylenemalonate (650 μL, 3.21 mmol) at 85°C for two hours, at 100°C for 18 hours and at 120°C for 3.3 hours. T.l.c. analysis (acetone : cyclohexane, 1:3) showed presence of one product (R_f 0.13) and consumption of both starting materials (R_f 0.32 and 0.46). The reaction solution was concentrated *in vacuo* to give diethyl 2-(((3-(difluoromethyl)phenyl)amino)methylene)malonate (1.00 g, quant.) as a dark yellow oil. **NMR Data** – 1H-NMR (400 MHz, CDCl$_3$): 11.0 (1H, d, $J_{NH,HE}$ 10.8 Hz, NH), 8.46 (1H, d, $J_{HE,NH}$ 10.8 Hz, H^E), 7.35 (1H, t, $^4J_{HA,CHF2}$ 6.8 Hz, H^A), 6.98 (1H, ddd, J 6.4, 1.6, 0.4 Hz, H^C), 6.91-6.88 (2H, m, H^B & H^D), 6.53 (1H, t, $^2J_{CH,F}$ 58.8 Hz, CHF$_2$), 4.31, 4.25 (2 x q, $J_{CH2,CH3}$ 5.6 Hz for both q, 2 x CH$_2$), 1.38, 1.33 (2 x t, $J_{CH3,CH2}$ 5.6 Hz for both t, 2 x CH$_3$). 13C-NMR (100 MHz, CDCl$_3$): 169.0, 165.5 (2 x C=O), 162.3 (Cq-CHF$_2$), 151.4 (CH^E), 140.9 (Cq-NH), 131.2 (CH^A), 115.7 (t, $^2J_{CH,F}$ 20.7 Hz, CHF$_2$), 115.4, 108.7 (CH^B, CH^D), 113.9 (CH^C), 94.7 (Cq-CH^E), 60.7, 60.3 (2 x CH$_2$), 14.5, 14.3 (2 x CH$_3$).

MS134A, diethyl 2-(((4-methoxyphenyl)amino)methylene)malonate

para-Anisidine (4-methoxyaniline) (2.01 g, 16.32 mmol) was stirred with diethyl ethoxymethylenemalonate (3.28 mL, 16.24 mmol) between 100 and 125°C for 18.5 hours. T.l.c. analysis (ethyl acetate : cyclohexane, 1:3) showed presence of one product (R_f 0.41) and consumption of both starting materials (R_f 0.32 and 0.49). The reaction solution was concentrated *in vacuo* to give diethyl 2-(((4-methoxyphenyl)amino)methylene)malonate (4.76 g, quant.) as a dark liquid. **NMR Data** – 1H-NMR (400 MHz, CDCl$_3$): 10.96 (1H, d, $J_{NH,HE}$ 13.7 Hz, NH), 8.41 (1H, d, $J_{HE,NH}$ 13.8 Hz, H^E), 7.05 (2H, d, $J_{HA,HB}$ 6.8 Hz, H^A), 6.88 (1H, d, $J_{HB,HA}$ 7.2 Hz, H^B), 4.27, 4.21 (2 x q, $J_{CH2,CH3}$ 5.6 Hz for both q, 2 x CH$_2$), 3.82 (3H, OCH$_3$), 1.35, 1.29 (2 x t, $J_{CH3,CH2}$ 5.6 Hz for both t, 2 x CH$_3$). 13C-NMR (100 MHz, CDCl$_3$): 169.3, 165.9 (2 x C=O), 157.2 (Cq-OCH$_3$), 152.7 (CH^E), 132.8 (Cq-NH), 118.8, 115.1 (CH^A, CH^B), 92.5 (Cq-CH^E), 60.3, 60.0 (2 x CH$_2$), 55.6 (OCH$_3$), 14.5, 14.4 (2 x CH$_3$). LCMS (ES+) 316 [M+Na]$^+$, 293.1 [MH]$^+$.

Virtual screening for analogues of MS131A was performed using the multifingerprint browser for the ZINC database (Awale and Reymond, 2014). Analogues were selected on the basis of the available five different similarity methods by clustering of the 1000 nearest neighbours in each case. Focusing on compounds available from Princeton Biomolecular Research, we obtained 61 compounds for experimental screening, which were purchased as 1 mg solid samples and conditioned as 10 mM stock solutions in DMSO for testing.

Materials, Cell culture and transfections

Unless otherwise stated, chemicals were purchased from Sigma Aldrich. VX-770 and VX-809 were purchased from Selleck Chemicals. P2 (PG-01; Pedemonte et al., 2005b), P5 (dF508act-02; Yang et al., 2003), and Corr-4a (4a; Pedemonte et al., 2005a) were obtained from the CFTR Chemical Compound Distribution Program, sponsored by the Cystic Fibrosis Foundation Therapeutics. HEK293 cells were maintained in DMEM, supplemented with 2 mM L-glutamine, 100 U/ml penicillin and streptomycin, and 10% FBS (all Life

Technologies). For fluorescence imaging, cells were seeded in poly-D-lysine (PDL)-coated, black walled 96-well plates (Costar, Fisher Scientific).

Lipofectamine transfection was used for all cells used for patch-clamp and imaging experiments. Cells plated in 96-well plates were transiently transfected with the appropriate YFP-CFTR- or CFTR-pHTomato- encoding plasmid using Lipofectamine 2000 (Life Technologies), according to manufacturer's instructions. Following transfection, cell plates were returned to the 37°C incubator for 24 h. Where indicated, plates were further incubated at 30°C for 24 h prior to imaging, with or without additional drug treatment.

Single channel patch-clamp recording

HEK293 cells in 35 mm dishes, expressing WT-CFTR or YFP-WT-CFTR, along with GFP as a marker of transfection, were used for voltage-clamp recording, in the excised inside-out patch configuration. Excised patch recordings were made using an EPC9 amplifier and Pulse acquisition software (HEKA Instruments Inc., MA, US). Cells were mounted in 35 mm dishes above an inverted fluorescence microscope (Nikon Eclipse TE200), with mercury light source and GFP filters (excitation/emission 450-500 nm/510-560 nm, dichroic mirror transmitted > 505 nm). Cells were continuously perfused with bath solution (134 mM NMDG, 134 mM HCl, 2 mM $MgCl_2$, 5 mM HEPES, 0.5 mM EGTA, pH 7.1). Pipette solution contained 136 mM NMDG, 136 mM HCl, 2 mM $MgCl_2$ and 5 mM HEPES (pH 7.4). Pipettes were pulled from borosilicate glass capillaries (Harvard Apparatus Ltd., Cambridge, UK) using a vertical pipette puller (Narishige PP-830, Digitimer Ltd.), were coated with Sylgard (Sigma-Aldrich), and fire polished on a microforge (Narishige MF-830, Digitimer). When filled with pipette solution, they typically had a resistance of around 12 MΩ.

The cytosolic face of the patch was continuously perfused using a gravity-driven microperfusion system. CFTR was activated by addition of 300 nM PKA (~100 U/ml catalytic subunit from bovine heart, Sigma-Aldrich P-2645) and 2 mM ATP for approximately 2 minutes in order to reach steady state phosphorylation. After this time, PKA was removed and recording continued in 2 mM ATP. No significant difference was found in the value of kinetic parameters obtained before and after PKA removal, consistent with a very slow dephosphorylation rate in this system. Continuous recordings were acquired at 5 kHz and pre-filtered at 1 kHz, at room temperature with the pipette potential held at + 60 mV (- 60 mV membrane potential).

Analysis of patch data

Records were exported to ClampFit (Molecular Devices), and filtered digitally at 50 Hz. Programs developed by László Csanády (Semmelweis University, Budapest) were used to analyse traces (Csanády, 2000). Briefly, the distributions of dwell-times at all conductance levels were jointly fit assuming a three-state gating model ($C_1 \leftrightarrow O \leftrightarrow C_2$), in which $C_1 \leftrightarrow O$ represents a simplified opening and closing (entry and exit from bursts), and $O \leftrightarrow C_2$ represents ATP-independent fast, flickery closures. Maximum Likelihood fitting provided estimates for opening rate (r_{CO}), closing rate (r_{OC}) and flicker rates (r_{OF} and r_{FO}: on and off rates of flicker closures, respectively) of the channel, and thus interburst duration ($\tau_{ib,} = 1/r_{CO}$), and open burst duration ($\tau_{b,} = (1/r_{OC})*(1+r_{OF}/r_{FO})$).

Both r_{CO} and r_{OC} can be reliably estimated when the number of channels in the patch is known. In most recordings the number of channels in the patch could not be estimated with sufficient confidence (see Vergani et al., 2003 for criteria used to determine whether number of channels in the patch was unknown). In these circumstances, noise analysis was used to estimate P_o. τ_b can still be estimated from dwell time distributions, as it is not steeply dependent on the number of channels. Therefore, when the number of channels in a patch could not be determined, P_o was obtained from noise analysis, τ_b from Maximum Likelihood fitting of dwell-time histograms, and τ_{ib} as

$$\tau_{ib} = \frac{\tau_b(1-P_o)}{P_o} \qquad \text{Equation [1]}$$

YFP-CFTR wide-field imaging

All imaging was carried out using ImageXpress (ImageXpress Micro XLS, Molecular Devices); an image-acquisition system equipped with wide-field inverted fluorescence microscope, CMOS camera and fluidics robotics. 96-well cell plates were contained in an environmental chamber, at 37°C or 30°C. YFP-CFTR was imaged using a 20X objective, and excitation/emission filters 472 ± 30 nm and 520 ± 35 nm. For each plate, the laser intensity and exposure were optimised to achieve the highest possible fluorescence whilst avoiding both photobleaching and saturation (illumination intensity 100-150/225 cd, and exposure 0.1 – 0.2 s)

Before imaging, cells were washed twice with 100 µl standard buffer (140 mM NaCl, 4.7 mM KCl, 1.2 mM MgCl$_2$, 5 mM HEPES, 2.5 mM CaCl$_2$, 1 mM Glucose, pH 7.4). Images

were taken for 150 s at a frequency of 0.5 Hz. 50 µl extracellular I^- (as standard buffer with 140 mM NaCl replaced with 300 mM NaI; resulting in 100 mM final $[I^-]$) was added at 20 s, and activating compounds were added at 60 s (in 100 mM I^-) at the concentrations indicated. For experiments in which extracellular $[I^-]$ was lower (Figure 1), the sum of [NaCl] and [NaI] was maintained at 140 mM.

YFP-CFTR confocal imaging

Confocal images were acquired using the Opera High Content Screening System (PerkinElmer Life and Analytical Sciences, Bucks., UK). Cells were washed as above, incubated with Hoechst nuclear stain, and imaged with a 40X objective at 37°C. YFP-CFTR imaging was carried out using a triple bandpass excitation filter (488/561/640 nm) and emission filter 540 ± 37.5 nm. Hoechst was excited by UV light and a 425 nm dichroic longpass mirror; emission filter was at 450 ± 25 nm.

CFTR-pHTomato imaging

Before imaging, cells were washed twice with 100 µl standard buffer (as above). During imaging, extracellular pH was changed using addition of 50 µl pH 6 buffer (as standard buffer, with 5 mM HEPES replaced with 10 mM MES: final [MES] 3.3 mM, final value ~ pH 6.5), and 50 µl pH 9 buffer (as standard buffer, with 5 mM HEPES replaced with 100 mM Tris: final [Tris] 25 mM, ~ pH 8.8). Two pHTomato images (acquisition frequency 0.5 Hz) were taken in each condition, using bandpass excitation/emission filters 531 ± 20 nm and 592 ± 20 nm. Single eGFP and Hoechst nuclear stain images were also acquired for each well, using excitation/emission filters 472 ± 30 nm and 520 ± 35 nm, and 377 ± 25 nm and 447 ± 30 nm, respectively.

Data analysis

Images were analysed using ImageJ (http://rsbweb.nih.gov/ij/). For each well, data were exported as a stack, with each time point represented by an image in the stack. For YFP-CFTR, image areas corresponding to transfected cells were selected, before addition of I^-, using a fluorescence threshold. Fluorescence was normalised to this maximal value. Very high extracellular $[I^-]$ allows accumulation of $[I^-]_{in}$ which completely quenches YFP-CFTR fluorescence intensity to background levels (Figure 1), confirming that anion binding abolishes fluorescence in our system. Thus fluorescence quenching can be described by an equation including a Hill-Langmuir component:

$$\frac{F}{F_{max}} = 1 - \frac{[I^-]_{in}}{K_I + [I^-]_{in}}$$ Equation [2]

Where $\frac{F}{F_{max}}$ is the normalised fluorescence, K_I is the dissociation constant for I^- binding to YFP (1.9 mM; Galietta et al., 2001a) and $[I^-]_{in}$ is the concentration of I^- at the chromophore. Experimentally, we can alter $[I^-]_{in}$ by increasing extracellular I^- concentration, $[I^-]_{out}$. The fact that we can describe the observed changes in fluorescence as a function of $[I^-]_{out}$ with equation [2] (Figure 1), suggests that membrane potential is not greatly affected by changes in $[I^-]_{out}$.

Equation [2] can be rearranged to express $[I^-]_{in}$ as a function of $\frac{F}{F_{max}}$:

$$[I^-]_{in} = K_I \frac{1 - \frac{F}{F_{max}}}{\frac{F}{F_{max}}}$$ Equation [3]

A plot of $[I^-]_{in}$ against time was used to calculate the maximal rate of I^- entry into cells ($d[I^-]/dt$, mM s^{-1}), which was then used to quantify CFTR activation (Figure 2).

The analysis as described above does not take into account the presence of cytosolic Cl^- ions, their binding to the chromophore at rest, and their displacement by I^- entering the cytosol. However, the discrepancy between the $[I^-]_{in}$ we calculate as above, assuming no competing anion, and that obtained assuming up to 20 mM cytosolic Cl^- (Bregestovski et al., 2009), is small (see S1, Supporting Information). To avoid introducing additional arbitrarily chosen parameters to describe the more complex system, we therefore analyse our data assuming no Cl^- competition, as likely done in previous publications exploiting the anion-sensitive YFP (Galietta et al., 2001b; Pedemonte et al., 2005b).

For CFTR-pHTomato, regions corresponding to transfected cells were selected based on eGFP fluorescence. For each selected region, the mean eGFP fluorescence (F_{green}) was used to normalise the mean pHTomato fluorescence (F_{red}), to allow for differences in transfection efficiency. A weighted average was then obtained, with each region weighted by cell count:

$$F_{pHTomato} = \frac{\sum\left(\frac{F_{red}}{F_{green}} \, cell\,count\right)}{\sum(cell\,count)}$$ Equation [4]

Dose-response curves were fitted using the Hill equation

$$y = y_0 + \frac{a[L]^{n_H}}{EC_{50}{}^{n_H} + [L]^{n_H}}$$

where n_H is the Hill coefficient, EC_{50} is the half maximal effective concentration, y_0 is the response measured in the absence of ligand, L is ligand and a is the amplitude of the curve. Where a value is not indicated, n_H is set to 1.

Statistical Analysis

All average plots including error bars represent mean ± SEM. In cases where two groups were compared, this was carried out using paired or unpaired t-test, as appropriate, or Mann-Whitney U test in cases where data was not normally distributed. Significance indicates $p < 0.05$. All statistical analysis was carried out using SigmaPlot (Systat Software).

Hit compounds from the pilot screen were identified using the strictly standardised mean difference (SSMD) score (Zhang et al., 2007; Zhang, 2011). The mean and standard deviation of the difference between the test and the negative reference was used to calculate one SSMD value which incorporated all replicates:

$$SSMD = \frac{\bar{d}_i}{\sqrt{0.5s_i^2 + 0.5s_o^2}}$$

Equation [5]

Where $\bar{d}_i$ is the mean of the differences between the test compound and negative reference, s_i^2 is the standard deviation of the same and s_o^2 is the median of all s_i^2 (Zhang, 2011). A combination of a common factor ($0.5s_0^2$), and the individual sample variance ($0.5s_i^2$) was used to stabilise the estimate of standard deviation due to the small n number (Zhang, 2011).

An SSMD value > 2 indicates a positive effect, consistently greater than the negative control (Zhang, 2011). Compounds with weak but very consistent effects will also have high SSMD values. To avoid selecting these compounds as hits, data were plotted on a dual-flashlight plot, in which SSMD is plotted against average percentage activation. Chosen hit compounds had SSMD > 2 and percentage activation $> 50\%$ of VX-770, and were therefore both statistically and biologically favourable (Zhang, 2011).

Results

The YFP-CFTR assay

Following the development of an anion sensitive YFP (H148Q/I152L) with optimal characteristics for CFTR research (Galietta et al., 2001a), a number of high-throughput screening projects have utilised cell-based assays in which soluble YFP is expressed in the cytosol (for examples see Galietta et al. 2001b; Pedemonte, et al. 2005b). Upon binding of halides, YFP fluorescence decreases (Jayaraman et al., 2000). Exploiting a high affinity for I^- compared to Cl^- (1.9 mM K_I vs. 85 mM K_{Cl}; Galietta et al. 2001a) Cl^-/I^- exchange protocols can report on CFTR function and, indirectly, on its membrane exposure.

We have engineered a YFP-CFTR fusion protein, in which YFP (H184Q/I152L) is fused to the N-terminal of CFTR. Expressed in HEK293 cells it forms the basis of an improved cell-based assay. Like in cytosolic YFP assays, in the presence of high extracellular $[I^-]$, and only if CFTR is present at the membrane and gating, I^- can enter the cell and quench YFP fluorescence. Normalised fluorescence values (Figure 2A) are converted to $[I^-]_{in}$ (Figure 2B), and CFTR activity is expressed in terms of the maximal rate of I^- entry into the cells (obtained from plots such as Figure 2C). Due to the direct correlation between YFP fluorescence intensity and levels of CFTR expression, normalising to fluorescence before addition of I^- (i.e. maximal fluorescence) accounts for variability in cellular expression of the probe, and reduces readout dispersion.

Using a high-content fluorescence microscope with fluidics capabilities (ImageXpress Micro XLS, Molecular Devices), we can identify and separately measure image areas corresponding to cells expressing YFP-CFTR as opposed to areas corresponding to "background". This allows sensitive, low-noise measurements of small, localised fluorescence changes triggered by fluid additions. Such measurements were used to construct a concentration-response curve to forskolin (Figure 2D). The forskolin EC_{50} obtained for YFP-WT-CFTR was similar to that obtained for WT-CFTR in a mouse mammary epithelial cell line (500 nM; Haws et al., 1996).

WT-CFTR vs. YFP-WT-CFTR

Published studies suggest that a GFP tag on the N-terminal of CFTR is not detrimental to either trafficking or function of the channel (Moyer et al., 1998; Vais et al., 2004; Ban et al., 2007). The similar forskolin EC_{50} of tagged and untagged CFTR confirms that an N-terminal YFP tag does not severely affect sensitivity to PKA-mediated phosphorylation. However, critical domain interactions have been ascribed to the N-tail (Naren et al., 1999; Chan et al., 2000; Fu et al., 2001).

To assess the effects of the YFP tag on CFTR gating kinetics, single-channel recording in the inside-out excised patch configuration was used to compare YFP-tagged and untagged WT-CFTR. P_o was reduced by the YFP tag to 64% that of WT-CFTR, mainly due to an increase in interburst duration (Figure 3). Thus the N-terminal YFP tag affects gating in a way comparable to a FLAG tag (Chan et al., 2000).

To investigate whether cellular distribution was affected, confocal images were obtained of HEK293 cells expressing YFP-WT-CFTR or YFP-F508del-CFTR. Images show mainly membrane localisation of YFP-WT-CFTR (Figure 4, white arrows), and internal, ER-like retention of YFP-F508del-CFTR (Figure 4, green arrows), as observed for untagged WT-CFTR and F508del-CFTR.

Overall, the mild functional alteration and expected cellular distribution confirmed suitability of the fusion protein for CFTR monitoring.

Known potentiators

Concentration-response curves to known potentiators were constructed using the YFP-F508del-CFTR assay (Figure 5), after temperature correction (24 h incubation at 30°C). P2 and P5 show the expected potency (Yang et al., 2003; Pedemonte et al., 2005b). The VX-770 EC_{50} we obtained (441 ± 144 nM, for F508del-CFTR) is higher than some of the published values, with EC_{50} values ranging from low nanomolar (Van Goor et al., 2009; Veit et al., 2014) to 129 ± 38 nM (Van Goor et al., 2014).

Figure 5 confirms that the YFP-F508del-CFTR assay is suitable for detecting potentiation. As the potentiator with the highest efficacy, VX-770 was chosen as the positive control for a pilot compound screen.

Pilot screen

A small library of 138 compounds was selected from UCL ChemiBank: a resource of diverse, drug-like compounds for screening (The Wolfson Institute for Biomedical Research, UCL, London). Compounds were selected on the basis of structural resemblance to VX-770, but also included some dissimilar chemical intermediates.

Test compounds were screened at 10 µM in triplicate, in the presence of 50 µM forskolin. Three compounds with SSMD > 2 and mean activity > 50% that of 10 µM VX-770 were identified (Figure 6A and 6B); the activity of two could be confirmed on YFP-F508del-CFTR and YFP-G551D-CFTR (Figures 6C). Concentration-response curves were obtained after all solutions (10 mM stock in DMSO and dilutions) were made freshly from solid stock to exclude the possibility of sample contamination. The third hit compound was not further investigated, as insolubility became a major obstacle. The confirmed active compounds, MS131A (chemical name, diethyl 2-(((3-(difluoromethoxy)phenyl)amino)methylene)malonate) and MS134A (chemical name, diethyl 2-(((4-methoxyphenyl)amino)methylene)malonate), were in fact chemical intermediates *en route* to cyclic structures and are quite dissimilar from VX-770 (Tanimoto similarity = 0.28).

Differences in compound efficacy when tested on F508del-CFTR vs. G551D-CFTR confirmed that the response detected in the screen was mediated by potentiation of CFTR, and not an alternative anion channel. Given the high structural similarity of the two hit compounds, further work was carried out only on one. MS131A was chosen due to marginally higher efficacy on F508del-CFTR compared to MS134A (Figure 6C).

The CFTR-pHTomato assay

The CFTR-pHTomato localisation assay exploits a pH sensitive, red fluorescent protein. Both the excitation and the emission spectra of pHTomato are strongly pH-dependent (pK_a ~7.8). As pH increases fluorescence increases, since only the deprotonated form is fluorescent (Li and Tsien, 2012).

In our assay, pHTomato is inserted within an extracellular loop of CFTR. This insertional fusion does not alter the pH-dependence of pHTomato (see Supporting Information Figure S2D). We chose a site following position 901 in extracellular loop 4, known to be a permissive site for tag insertion on CFTR (Howard et al., 1995; Schultz et al., 1997; Sharma et al., 2001; Hildebrandt et al., 2015). Even a relatively large tag (308 amino

acid Horseradish Peroxidase; HRP) at this position in F508del-CFTR has been shown not to alter drug responses or cellular localisation (Phuan et al., 2014).

CFTR-pHTomato is expressed in HEK293 cells. Transient transfection of cells has variable efficiency, resulting in variable levels of protein expression in individual cells. To reduce such variability, CFTR-pHTomato and eGFP are encoded on a pIRES2 plasmid: a single, bicistronic mRNA is transcribed in cells, from which translation of both proteins occurs. Assay readout is obtained as fluorescence on the red channel divided by that on the green channel. Therefore, such readouts reflect steady state levels of CFTR-pHTomato, a complex function of biosynthetic, trafficking and degradation rates, but independent of transfection efficiency (Supporting Information, S2).

Image acquisition begins in pH 6 buffer (Figure 7A (*i*)). The fluorescence of membrane localised CFTR-pHTomato, exposed to pH 6, is only ~5% of maximal, and, because the pH of biosynthetic vesicle lumen is low (varies from neutral to pH 5; Wu et al., 2001), fluorescence from immature CFTR-pHTomato is also low. The extracellular pH is then changed to pH 9, using a non-permeant buffer. The increase in fluorescence intensity corresponding to this extracellular buffer change (ΔF_M) represents membrane-localised CFTR-pHTomato, as only CFTR-pHTomato located at the plasma membrane is exposed to the basic extracellular environment (Figure 7A (*ii*)). The final step adds 40 mM NH_4Cl, still maintaining extracellular pH 9 (Figure 7A (*iii*)). NH_3 permeates membranes and raises the pH of internal vesicles, increasing fluorescence of internal CFTR (Li and Tsien, 2012; Xu et al., 2014). The change in fluorescence at this final step (ΔF_IN) is used to estimate the level of immature CFTR-pHTomato localised along the biosynthetic pathway. ΔF_M and ΔF_IN are then used to estimate membrane and internal pools of WT-CFTR and F508del-CFTR (Figure 7B).

Known Correctors

Concentration-response curves were obtained for VX-809 and Corr-4a, after temperature correction at 30°C to enhance the F508del-CFTR-pHTomato signal. Both correctors increased membrane-localised CFTR in a concentration-dependent manner (Figure 8A). The EC_{50} values we obtained were similar to published values (Pedemonte et al., 2005a; Van Goor et al., 2011). Maximal correction by VX-809 is ~2-fold greater than that which is achieved by Corr-4a, also consistent with published data (Farinha et al., 2013; He et al., 2013; Okiyoneda et al., 2013). In addition, while we could not detect a relationship between the

concentration of Corr-4a and internal F508del-CFTR, VX-809 incubation caused a concentration-dependent increase in the levels of immature protein (Figure 8B), as well as well as of levels of plasma-membrane exposed protein.

Effects of chronic potentiator treatment on F508del-CFTR

CFTR-pHTomato was used to measure membrane destabilisation of F508del-CFTR caused by chronic treatment with potentiators. Membrane-localised F508del-CFTR, rescued by 10 μM VX-809 and 30°C incubation, was decreased by ~20% following 24 h incubation with 10 μM VX-770. There was no significant change in internal CFTR (Figure 9A). In contrast, MS131A had no significant effect on F508del-CFTR levels, after rescue by 10 μM VX-809 and low temperature (Figure 9B). In addition, at the end of the 24 h incubation, bound MS131A still potentiates gating (Figure 9C), ruling out the possibility that the lack of F508del-CFTR destabilisation might be caused by compound degradation during chronic incubation.

10 μM MS131A did not cause significant cell death during chronic incubation (DMSO control 0.9% ± 0.2% vs. 10 μM MS131A 1.7% ± 0.5%, n = 12, measured using NucGreen Dead 488 (Molecular Probes)), suggesting cell toxicity of the compound is low.

Discussion

YFP-CFTR functional assay can be used to identify F508del-CFTR potentiators

Effective pharmacological treatment of F508del-CF requires novel potentiators, devoid of the negative effects on biogenesis and stability that have been reported for almost all known F508del-CFTR potentiators (Cholon et al., 2014; Veit et al., 2014). This paper describes a pilot screen using the YFP-CFTR assay, capable of sensitive CFTR functional measurements. The presence of the fused N-terminal YFP has relatively minor effects on the gating function and cellular localisation of CFTR (Figure 3 and Figure 4), similar to what has been previously described for GFP-CFTR (Moyer et al., 1998; Vais et al., 2004; Ban et al., 2007). Our estimates of P2 and P5 potency confirmed published EC_{50} values (Yang et al., 2003; Pedemonte et al., 2005b), and in our assay VX-770 appeared to be only slightly less potent than previously reported (Van Goor et al., 2009; Veit et al., 2014, Van Goor et al., 2014). We cannot rule out that the YFP tag could alter the binding of VX-770, slightly reducing the apparent affinity, but minor cell-specific differences in expression of CFTR-interacting proteins and/or lipids are also possibilities.

A pilot screen of 138 compounds identified two novel potentiator compounds, whose activity was confirmed on F508del-CFTR and G551D-CFTR (Figure 6C). Our original intention was to screen compounds similar to VX-770, however, serendipitously, we observed potentiation with chemical intermediates MS131A and MS134A with dissimilar structures i.e. lacking the quinolone sub-structure of VX-770. It is interesting to note that the time course of activation by VX-770 and by the novel compounds also differs. After addition of forskolin (adenylate cyclase activator) and VX-770 quenching occurs only after a delay, consistent with activation requiring a build-up of cAMP levels followed by PKA-catalysed phosphorylation. However, upon addition of forskolin + MS131A quenching is immediate. More research will be necessary to determine whether this is due to the new compound not requiring prior phosphorylation, or an alternative mechanism.

CFTR-pHTomato assay

We also introduce the CFTR-pHTomato assay, a novel membrane-localisation assay capable of estimating membrane and internal CFTR, independent of channel function, in a rapid and inexpensive manner (Figure 7). Recently published assays have overcome the immediate need for techniques to quantify F508del-CFTR localisation without relying on channel function (Carlile et al., 2007; Botelho et al., 2015; Larsen et al., 2016). Like CFTR-pHTomato, each of these assays has advantages and limitations. One advantage of CFTR-pHTomato is that it does not require incubation with antibodies or other relatively expensive compounds. Used alongside a protein synthesis inhibitor, CFTR-pHTomato assays could be used − as a rapid and cheap alternative to pulse-chase experiments − to investigate altered stability at the plasma membrane of mutant CFTR. A reduced membrane half-life is one of the consequences of the F508del mutation (Lukacs et al., 1993), so rapid quantification of this parameter could be valuable in drug discovery projects. However, due to the inefficient folding and low peripheral stability, the levels of uncorrected F508del-CFTR protein at the plasma membrane are extremely low. This results in a very low signal for the pHTomato assay, and a signal:noise ratio that is not as high as with chemiluminescence.

The assay was validated using concentration-response curves to known corrector compounds (Figure 8). To enhance the fluorescence signal, these analyses were carried out on temperature-corrected F508del-CFTR. Consistent with our data (Figure 8B), VX-809 has been shown to stabilise F508del-CFTR during folding, to increase both the internal and membrane-localised pools of protein, whereas Corr-4a is understood to stabilise only

F508del-CFTR located at the membrane (Farinha et al., 2015, but also see Bali et al., 2016). The similarity of our observations to published data suggests that the pHTomato tag, like other tags at this location (Howard et al., 1995; Schultz et al., 1997; Phuan et al., 2014), does not severely alter cellular trafficking or drug mechanisms.

F508del-CFTR destabilisation by chronic potentiator treatment

Destabilisation of membrane-localised F508del-CFTR by chronic VX-770 treatment was confirmed using the CFTR-pHTomato assay (Figure 9A). Chronic treatment with 10 µM novel potentiator MS131A did not decrease membrane or internal F508del-CFTR in the CFTR-pHTomato assay (Figure 9B) and we could exclude that the activity was lost due to compound degradation during incubation (Figure 9C). Thus MS131A, like compounds based on potentiator P5 (Phuan et al., 2015), can potentiate F508del-CFTR without causing membrane destabilisation.

Further studies will be required to determine whether the two ester bonds in MS131A (Figure 6B), susceptible to hydrolysis catalysed by esterases present in the plasma, the intestine and the liver (Oda et al., 2015), can be replaced without affecting activity. A preliminary screening of 61 analogues of MS131A selected by virtual screening of commercial catalogues using substructure and pharmacophore similarity searches (Awale et al., 2015; Reymond, 2015) identified seven active compounds featuring variation of MS131A with different substituents on the aromatic ring but conserving the problematic malonic diester moiety.

Conclusions

YFP-CFTR and CFTR-pHTomato are novel fluorescence assays, capable of quantifying the defects associated with F508del-CFTR: reduced open probability and reduced membrane exposure. Using these assays, we could identify a novel compound with potentiator action, which did not cause destabilisation of F508del-CFTR following chronic incubation. Further structure-activity relationship studies would be required to improve potency and drug-like qualities. In addition, although the insertion of relatively large tags both at the N-terminal end and in the 4th extracellular loop has been shown to affect processing and function of CFTR and F508del-CFTR only to a small extent (see Moyer et al., 1998; Vais et al., 2004; Ban et al., 2007, and Howard et al., 1995; Schultz et al., 1997;

Hildebrandt et al., 2015, and Figures 2D, 3 and 4), mutation and/or drug effects identified with our assays would need to be confirmed using unmodified CFTR targets.

The pHTomato assay could be exploited for other protein trafficking diseases, the only requirement being a suitable extracellular domain to which the pHTomato can be tagged. One obvious protein, related to CFTR, whose cellular localisation is an important determinant of disease severity is ABCA4, an ABC transporter mutated in Stargardt disease (Sabirzhanova et al., 2015).

One of the weaknesses of the assays presented here is the cell line (HEK293) in which the fusion proteins are expressed. While, *in vivo*, CFTR is expressed apically in polarised epithelial cells, HEK293 cells do not form polarised monolayers, with high transepithelial resistance. In addition, CFTR folding and trafficking are complex processes, dependent on many accessory proteins, some of which are likely to be cell-type specific. Indeed, corrector mechanisms have shown cell-type specificity (Pedemonte et al., 2010; Farinha et al., 2015). For many drug-discovery projects, a cell line that more accurately represents the *in vivo* environment might be preferable. On the other hand, the flexibility and ease-of-use, high levels of expression, and low background signal obtained with our HEK293-based assays are advantages that might prove preferable if rapid and cheap testing of hypotheses is required (e.g. for the initial phases of projects investigating cell biology processes and/or drug mechanisms).

Author Contributions

Experiments were conceived and designed by EL, DLS and PV. EL carried out the molecular biology, ran the fluorescence assay acquisition and image analysis, and performed the patch-clamp experiments. DS provided the compound library for the pilot screen, MIS prepared MS131A and MS134A. JLR and CMSD performed the virtual screening to identify MS131A analogues. Manuscript was written by EL and PV. All authors read and commented on the final draft of the manuscript.

acquisition and analysis, and Dr László Csanády, Semmelweis University, for very interesting discussions.

Conflict of interest declaration

The authors declare no conflicts of interest.

References

Awale, M., Jin, X., and Reymond, J.-L. (2015). Stereoselective virtual screening of the ZINC database using atom pair 3D-fingerprints. J. Cheminform. *7*: 3.

Awale, M., and Reymond, J.L. (2014). A multi-fingerprint browser for the ZINC database. Nucleic Acids Res. *42*: 234–239.

Bali, V., Lazrak, A., Guroji, P., Matalon, S., and Bebok, Z. (2016). Mechanistic Approaches to Improve Correction of the Most Common Disease-Causing Mutation in Cystic Fibrosis. PLoS One *11*: e0155882.

Ban, H., Inoue, M., Griesenbach, U., Munkonge, F., Chan, M., Iida, A., et al. (2007). Expression and maturation of Sendai virus vector-derived CFTR protein□ : functional and biochemical evidence using a GFP-CFTR fusion protein. Gene Ther. *14*: 1688–1694.

Bompadre, S.G., Sohma, Y., Li, M., and Hwang, T.-C. (2007). G551D and G1349D, two CF-associated mutations in the signature sequences of CFTR, exhibit distinct gating defects. J. Gen. Physiol. *129*: 285–298.

Botelho, H.M., Uliyakina, I., Awatade, N.T., Proença, M.C., Tischer, C., Sirianant, L., et al. (2015). Protein Traffic Disorders: an Effective High-Throughput Fluorescence Microscopy Pipeline for Drug Discovery. Sci. Rep. *5*: 9038.

Bregestovski, P., Waseem, T., and Mukhtarov, M. (2009). Genetically encoded optical sensors for monitoring of intracellular chloride and chloride-selective channel activity. Front. Mol. Neurosci. *2*: 15.

Carlile, G.W., Robert, R., Zhang, D., Teske, K.A., Luo, Y., Hanrahan, J.W., et al. (2007). Correctors of protein trafficking defects identified by a novel high-throughput screening assay. Chembiochem *8*: 1012–1020.

Chan, K.W., Csanády, L., Seto-young, D., Nairn, A.C., and Gadsby, D.C. (2000). Severed Molecules Functionally Define the Boundaries of the Cystic Fibrosis Transmembrane Conductance Regulator's NH2 -terminal Nucleotide Binding Domain. J. Gen. Physiol. *116*: 163–180.

Cheng, S.H., Gregory, R.J., Marshall, J., Paul, S., Souza, D.W., White, G.A., et al. (1990). Defective intracellular transport and processing of CFTR is the molecular basis of most cystic fibrosis. Cell *63*: 827–834.

Cholon, D.M., Quinney, N.L., Fulcher, M.L., Charles, R.E.J., Das, J., Dokholyan, N. V, et al. (2014). Potentiator ivacaftor abrogates pharmacological correction of D F508 CFTR in cystic fibrosis. Sci. Transl. Med. *6*: 246ra96.

Csanády, L. (2000). Rapid kinetic analysis of multichannel records by a simultaneous fit to all dwell-time histograms. Biophys. J. *78*: 785–799.

Dalemans, W., Barbry, P., Champigny, G., Jallat, S., Dott, K., Dreyer, D., et al. (1991). Altered chloride ion channel kinetics associated with the deltaF508 cystic fibrosis mutation. Nature *354*: 526–528.

Davies, J.C., Wainwright, C.E., Canny, G.J., Chilvers, M.A., Howenstine, M.S., Munck, A., et al. (2013). Efficacy and safety of Ivacaftor in patients aged 6 to 11 years with cystic fibrosis with a G155D mutation. Am. J. Respir. Crit. Care Med. *187*: 1219–1225.

Denning, G.M., Anderson, M.P., Amara, J.F., Marshall, J., Smith, A.E., and Welsh, M.J. (1992). Processing of mutant cystic fibrosis transmembrane conductance regulator is temperature-sensitive. Nature *358*: 761–764.

Farinha, C.M., King-Underwood, J., Sousa, M., Correia, A.R., Henriques, B.J., Roxo-Rosa, M., et al. (2013). Revertants, Low Temperature, and Correctors Reveal the Mechanism of F508del-CFTR Rescue by VX-809 and Suggest Multiple Agents for Full Correction. Chem. Biol. *20*: 943–955.

Farinha, C.M., Sousa, M., Canato, S., Schmidt, A., Uliyakina, I., and Amaral, M.D. (2015). Increased efficacy of VX-809 in different cellular systems results from an early stabilization effect of F508del-CFTR. Pharmacol. Res. Perspect. *3*: e00152.

Flume, P.A., Liou, T.G., Borowitz, D.S., Li, H., Yen, K., Ordoñez, C.L., et al. (2012). Ivacaftor in subjects with cystic fibrosis who are homozygous for the F508del-CFTR mutation. Chest *142*: 718–724.

Fu, J., Ji, H.L., Naren, A.P., and Kirk, K.L. (2001). A cluster of negative charges at the amino terminal tail of CFTR regulates ATP-dependent channel gating. J. Physiol. *536*: 459–470.

Galietta, L.J., Haggie, P.M., and Verkman, A.S. (2001a). Green fluorescent protein-based halide indicators with improved chloride and iodide affinities. FEBS Lett. *499*: 220–224.

Galietta, L.J., Springsteel, M.F., Eda, M., Niedzinski, E.J., By, K., Haddadin, M.J., et al. (2001b). Novel CFTR chloride channel activators identified by screening of combinatorial libraries based on flavone and benzoquinolizinium lead compounds. J. Biol. Chem. *276*: 19723–19728.

Gregory, R.J., Rich, D.P., Cheng, S.H., Souza, D.W., Paul, S., Manavalan, P., et al. (1991). Maturation and function of cystic fibrosis transmembrane conductance regulator variants bearing mutations in putative nucleotide-binding domains 1 and 2. Mol. Cell. Biol. *11*: 3886–3893.

Haws, C.M., Nepomuceno, I.B., Krouse, M.E., Wakelee, H., Law, T., Xia, Y., et al. (1996). Delta F508-CFTR channels □ : kinetics , activation by forskolin , and potentiation by xanthines. Am. J. Physiol. Cell Physiol. *270*: C1544-1555.

He, L., Kota, P., Aleksandrov, A.A., Cui, L., Jensen, T., Dokholyan, N. V, et al. (2013). Correctors of ΔF508 CFTR restore global conformational maturation without thermally stabilizing the mutant protein. FASEB J. *27*: 536–545.

Hildebrandt, E., Ding, H., Mulky, A., Dai, Q., Aleksandrov, A.A., Bajrami, B., et al. (2015). A Stable Human-Cell System Overexpressing Cystic Fibrosis Transmembrane Conductance

Regulator Recombinant Protein at the Cell Surface. Mol. Biotechnol. *57*: 391–405.

Howard, M., DuVall, M.D., Devor, D.C., Dong, J.Y., Henze, K., and Frizzell, R.A. (1995). Epitope tagging permits cell surface detection of functional CFTR. Am. J. Physiol. *269*: C1565-1576.

Jayaraman, S., Haggie, P., Wachter, R.M., Remington, S.J., and Verkman, A.S. (2000). Mechanism and cellular applications of a green fluorescent protein-based halide sensor. J. Biol. Chem. *275*: 6047–6050.

Larsen, M.B., Hu, J., Frizzell, R.A., and Watkins, S.C. (2016). Simple image-based no-wash method for quantitative detection of surface expressed CFTR. Methods *96*: 40–45.

Li, Y., and Tsien, R.W. (2012). pHTomato, a red, genetically encoded indicator that enables multiplex interrogation of synaptic activity. Nat. Neurosci. *15*: 1047–1053.

Lukacs, G.L., Chang, X.B., Bear, C.E., Kartner, N., Mohamed, a, Riordan, J.R., et al. (1993). The DF508 mutation decreases the stability of cystic fibrosis transmembrane conductance regulator in the plasma membrane. J Biol Chem *268*: 21592–21598.

Lukacs, G.L., and Verkman, A.S. (2012). CFTR: folding, misfolding and correcting the ΔF508 conformational defect. Trends Mol. Med. *18*: 81–91.

Matthes, E., Goepp, J., Carlile, G.W., Luo, Y., Dejgaard, K., Billet, A., et al. (2016). Low free drug concentration prevents inhibition of F508del CFTR functional expression by the potentiator VX-770 (ivacaftor). Br. J. Pharmacol. *173*: 459–470.

Miki, H., Zhou, Z., Li, M., Hwang, T.-C., and Bompadre, S.G. (2010). Potentiation of disease-associated cystic fibrosis transmembrane conductance regulator mutants by hydrolyzable ATP analogs. J. Biol. Chem. *285*: 19967–19975.

Moyer, B.D., Loffing, J., Schwiebert, E.M., Loffing-Cueni, D., Halpin, P.A., Karlson, K.H., et al. (1998). Membrane Trafficking of the Cystic Fibrosis Gene Product , Cystic Fibrosis Transmembrane Conductance Regulator , Tagged with Green Fluorescent Protein in Madin-Darby Canine Kidney Cells. J. Biol. Chem. *273*: 21759–21768.

Naren, A.P., Cormet-Boyaka, E., Fu, J., Villain, M., Blalock, J.E., Quick, M.W., et al. (1999). CFTR Chloride Channel Regulation by an Interdomain Interaction. Science (80-.). *286*: 544–548.

Oda, S., Fukami, T., Yokoi, T., and Nakajima, M. (2015). A comprehensive review of UDP-glucuronosyltransferase and esterases for drug development. Drug Metab. Pharmacokinet. *30*: 30–51.

Okiyoneda, T., Barrière, H., Bagdány, M., Rabeh, W.M., Du, K., Höhfeld, J., et al. (2010). Peripheral protein quality control removes unfolded CFTR from the plasma membrane. Science *329*: 805–810.

Okiyoneda, T., Veit, G., Dekkers, J.F., Bagdany, M., Soya, N., Xu, H., et al. (2013). Mechanism-based corrector combination restores deltaF508-CFTR folding and function. Nat. Chem. Biol. *9*: 444–454.

Pedemonte, N., Lukacs, G.L., Du, K., Caci, E., Zegarra-moran, O., Galietta, L.J. V, et al. (2005a). Small-molecule correctors of defective Δ F508-CFTR cellular processing identified

by high-throughput screening. J. Clin. Invest. *115*: 2564–2571.

Pedemonte, N., Sonawane, N.D., Taddei, A., Hu, J., Zegarra-moran, O., Suen, Y.F., et al. (2005b). Phenylglycine and Sulfonamide Correctors of Defective delF508 and G551D Cystic Fibrosis Transmembrane Conductance Regulator Chloride-Channel Gating. Mol. Pharmacol. *67*: 1797–1807.

Pedemonte, N., Tomati, V., Sondo, E., and Galietta, L.J. V (2010). Influence of cell background on pharmacological rescue of mutant CFTR. Am. J. Physiol. Cell Physiol. *298*: C866-874.

Phuan, P.-W., Veit, G., Tan, J., Finkbeiner, W.E., Lukacs, G.L., and Verkman, A.S. (2015). Potentiators of Defective ΔF508-CFTR Channel Gating that do not Interfere with Corrector Action. Mol. Pharmacol. *88*: 791–799.

Phuan, P.-W., Veit, G., Tan, J., Roldan, A., Finkbeiner, W.E., Lukacs, G., et al. (2014). Synergy-based Small-Molecule Screen Using a Human Lung Epithelial Cell Line Yields F508-CFTR Correctors that Augment VX-809 Maximal Efficacy. Mol. Pharmacol. *86*: 42–51.

Ramsey, B.W., Davies, J., McElvaney, N.G., Tullis, E., Bell, S.C., Dřevínek, P., et al. (2011). A CFTR Potentiator in Patients with Cystic Fibrosis and the G155D mutation. N. Engl. J. Med. *365*: 1663–1672.

Reymond, J.L. (2015). The Chemical Space Project. Acc. Chem. Res. *48*: 722–730.

Riordan, J.R., Rommens, J.M., Kerem, B., Alon, N., Rozmahel, R., Grzelczak, Z., et al. (1989). Identification of the cystic fibrosis gene: cloning and characterization of complementary DNA. Science *245*: 1066–1073.

Rowe, S.M., and Verkman, A.S. (2013). Cystic fibrosis transmembrane regulator correctors and potentiators. Cold Spring Harb. Perspect. Med. *3*:.

Sabirzhanova, I., Lopes Pacheco, M., Rapino, D., Grover, R., Handa, J.T., Guggino, W.B., et al. (2015). Rescuing trafficking mutants of the ATP-binding cassette protein, ABCA4, with small molecule correctors as a treatment for Stargardt eye disease. J. Biol. Chem. *290*: 19743–19755.

Schultz, B.D., Takahashi, A., Liu, C., Frizzell, R.A., and Howard, M. (1997). FLAG epitope positioned in an external loop preserves normal biophysical properties of CFTR. Am. J. Physiol. *273*: C2080-2089.

Sharma, M., Benharouga, M., Hu, W., and Lukacs, G.L. (2001). Conformational and temperature-sensitive stability defects of the delta F508 cystic fibrosis transmembrane conductance regulator in post-endoplasmic reticulum compartments. J. Biol. Chem. *276*: 8942–8950.

Vais, H., Gao, G.-P., Yang, M., Tran, P., Louboutin, J.-P., Somanathan, S., et al. (2004). Novel adenoviral vectors coding for GFP-tagged wtCFTR and deltaF508-CFTR: characterization of expression and electrophysiological properties in A549 cells. Pflugers Arch. *449*: 278–287.

Van Goor, F., Hadida, S., Grootenhuis, P.D.J., Burton, B., Cao, D., Neuberger, T., et al. (2009). Rescue of CF airway epithelial cell function in vitro by a CFTR potentiator, VX-770.

Proc. Natl. Acad. Sci. U. S. A. 106: 18825–18830.

Van Goor, F., Hadida, S., Grootenhuis, P.D.J., Burton, B., Stack, J.H., Straley, K.S., et al. (2011). Correction of the F508del-CFTR protein processing defect in vitro by the investigational drug VX-809. Proc. Natl. Acad. Sci. U. S. A. 108: 18843–18848.

Van Goor, F., Yu, H., Burton, B., and Hoffman, B.J. (2014). Effect of ivacaftor on CFTR forms with missense mutations associated with defects in protein processing or function. J. Cyst. Fibros. 13: 29–36.

Veit, G., Avramescu, R.G., Perdomo, D., Phuan, P.-W., Bagdany, M., Apaja, P.M., et al. (2014). Some gating potentiators, including VX-770, diminish F508-CFTR functional expression. Sci. Transl. Med. *6*: 246ra97.

Vergani, P., Nairn, A.C., and Gadsby, D.C. (2003). On the Mechanism of MgATP-dependent Gating of CFTR Cl- Channels. J. Gen. Physiol. *120*: 17–36.

Wainwright, C.E., Elborn, J.S., Ramsey, B.W., Marigowda, G., Huang, X., Cipolli, M., et al. (2015). Lumacaftor–Ivacaftor in Patients with Cystic Fibrosis Homozygous for Phe508del CFTR. N. Engl. J. Med. *373*: 220–231.

Ward, C.L., Omura, S., and Kopito, R.R. (1995). Degradation of CFTR by the ubiquitin-proteasome pathway. Cell *83*: 121–7.

Wu, M.M., Grabe, M., Adams, S., Tsien, R.Y., Moore, H.P.H., and Machen, T.E. (2001). Mechanisms of pH Regulation in the Regulated Secretory Pathway. J. Biol. Chem. *276*: 33027–33035.

Xu, J., Chai, H., Ehinger, K., Egan, T.M., Srinivasan, R., Frick, M., et al. (2014). Imaging P2X4 receptor subcellular distribution, trafficking, and regulation using P2X4-pHluorin. J. Gen. Physiol. *144*: 81–104.

Yang, H., Shelat, A.A., Guy, R.K., Gopinath, V.S., Ma, T., Du, K., et al. (2003). Nanomolar affinity small molecule correctors of defective Delta F508-CFTR chloride channel gating. J. Biol. Chem. *278*: 35079–35085.

Yu, H., Burton, B., Huang, C.-J., Worley, J., Cao, D., Johnson, J.P., et al. (2012). Ivacaftor potentiation of multiple CFTR channels with gating mutations. J. Cyst. Fibros. *11*: 237–245.

Zhang, X.D. (2011). Illustration of SSMD, z score, SSMD*, z* score, and t statistic for hit selection in RNAi high-throughput screens. J. Biomol. Screen. *16*: 775–785.

Zhang, X.D., Ferrer, M., Espeseth, A.S., Marine, S.D., Stec, E.M., Crackower, M.A., et al. (2007). The use of strictly standardized mean difference for hit selection in primary RNA interference high-throughput screening experiments. J. Biomol. Screen. Off. J. Soc. Biomol. Screen. *12*: 497–509.

UK CF Registry annual report (2015). https://www.cysticfibrosis.org.uk/the-work-we-do/uk-cf-registry/reporting-and-resources
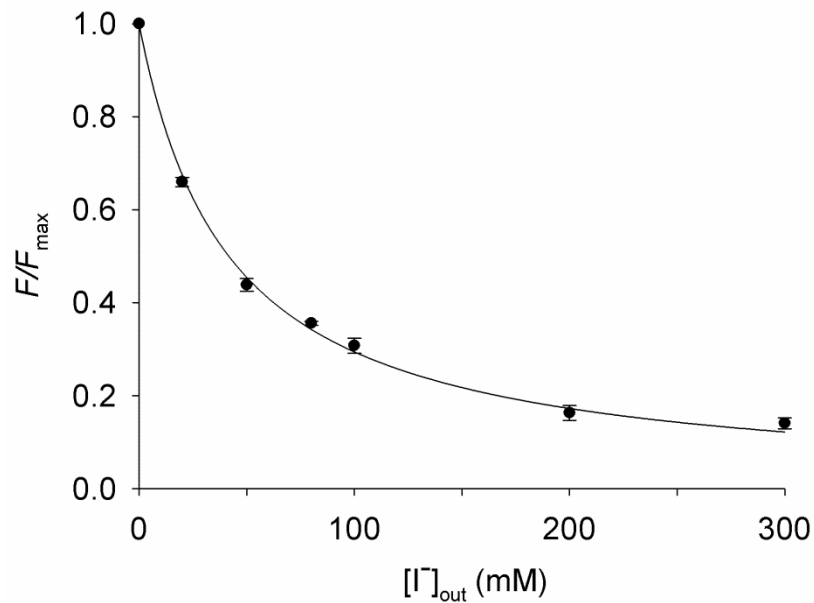
Figure 1. Steady state fluorescence measured at increasing $[I^-]_{out}$. Solid line is a fit to equation [2], but using $[I^-]_{out}$ as the independent variable. The apparent K_I obtained is 41.4 ± 1.3 mM. At a membrane potential of -83 mV, $[I^-]_{out} = 41.4$ mM is in equilibrium with $[I^-]_{in} = 1.9$ mM. Alternatively, at a membrane potential of -77.5 mV, $[I^-]_{out} = 41.4$ mM is in equilibrium with $[I^-]_{in} = 2.35$ mM, effective half-maximal $[I^-]_{in}$, assuming a $[Cl^-]_{in} = 20$ mM. $n = 3$ wells from 1 experiment.
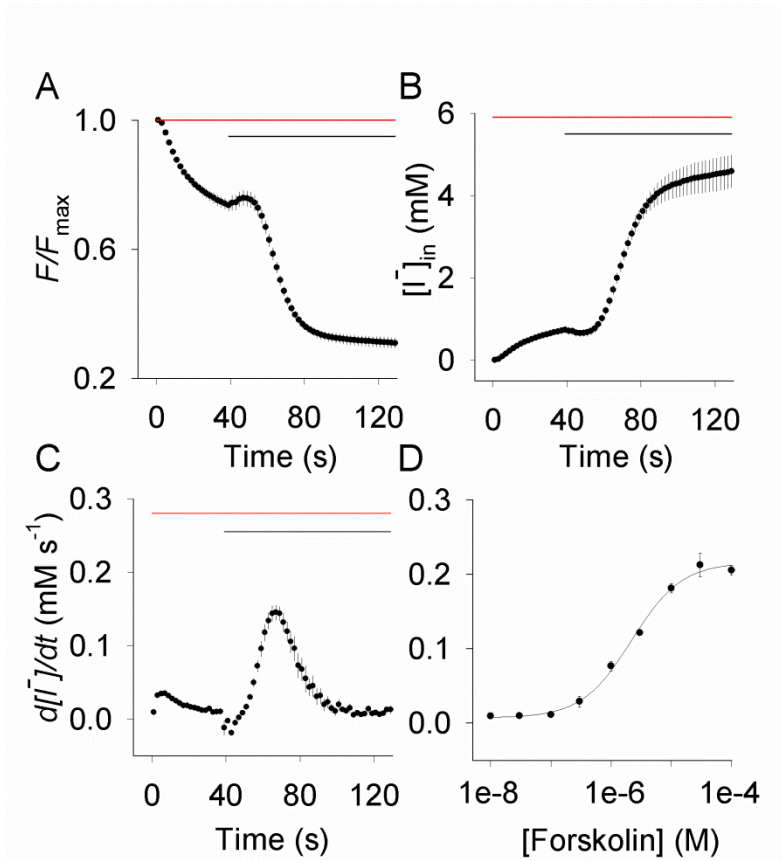
Figure 2. Quantification of CFTR ion channel function using YFP-CFTR. A) YFP-WT-CFTR fluorescence quenching in response to addition of 100 mM extracellular I^- (red bar) and of 20 μM forskolin (adenylate cyclase activator, black bar). B) $[I^-]_{in}$ increase. C) The gradient of the trace in B) gives the rate of I^- entry at each time point. D) Forskolin concentration-response curve of WT-CFTR using maximal observed I^- entry rate ($d[I^-]/dt$, mM s^{-1}) to quantify CFTR activation. $EC_{50} = 2.2$ μM $\pm$ 0.3 μM. n = 3 wells from 1 experiment.
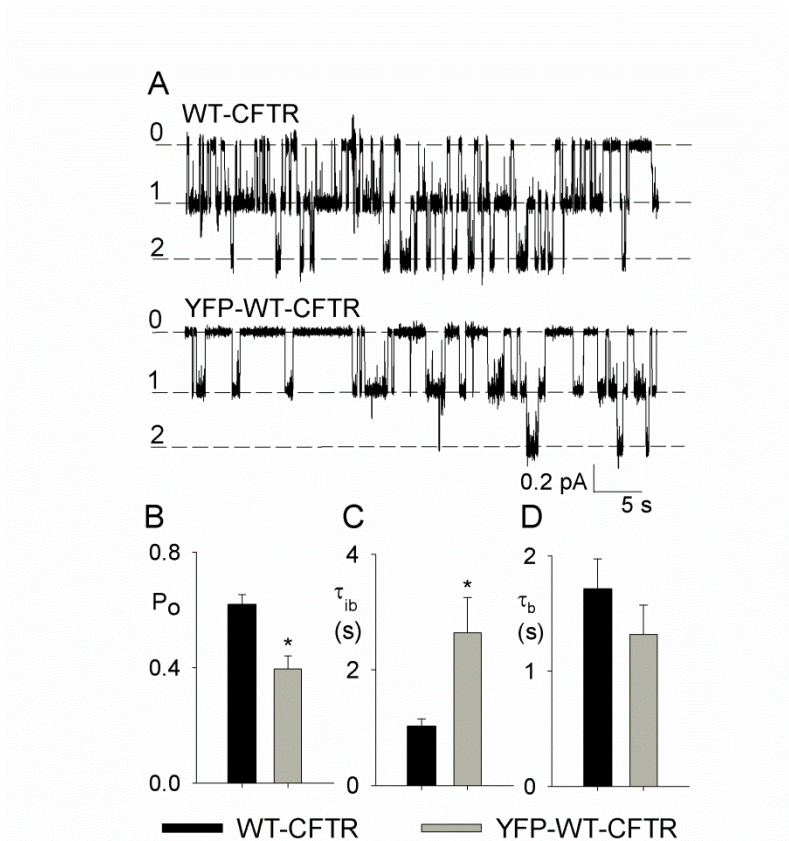
Figure 3. Gating of WT-CFTR and YFP-WT-CFTR expressed in HEK293 cells. A) Representative excised patch recordings of WT-CFTR and YFP-WT-CFTR containing two gating channels in the presence of 2 mM ATP, following exposure to 300 nM PKA. Dashed lines: current levels corresponding to 0, 1 or 2 open channels. B) Open probability C) Interburst duration and D) Burst duration, derived from noise analysis and dwell-time distribution analysis. n = 11 and 15 for tagged and untagged, respectively. * $p < 0.05$ from Mann-Whitney U test.
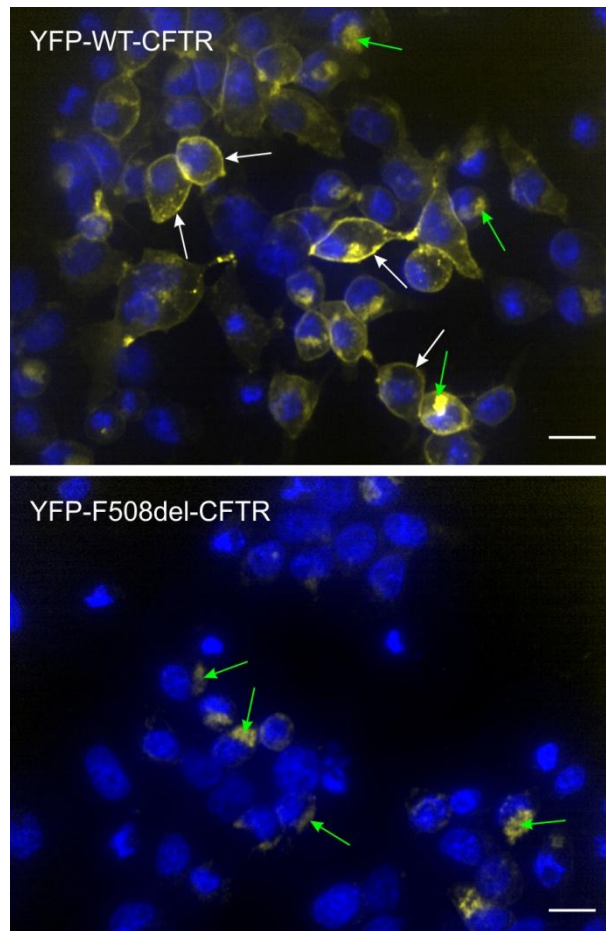
Figure 4. YFP-WT-CFTR and YFP-F508del-CFTR localisation. Confocal images of HEK293 cells expressing YFP-WT-CFTR (top panel) or YFP-F508del-CFTR (bottom panel). White arrows indicate membrane localisation, green arrows indicate intracellular retention. Yellow = YFP-CFTR, blue = Hoechst nuclear stain. Scale bar = 10 μm.
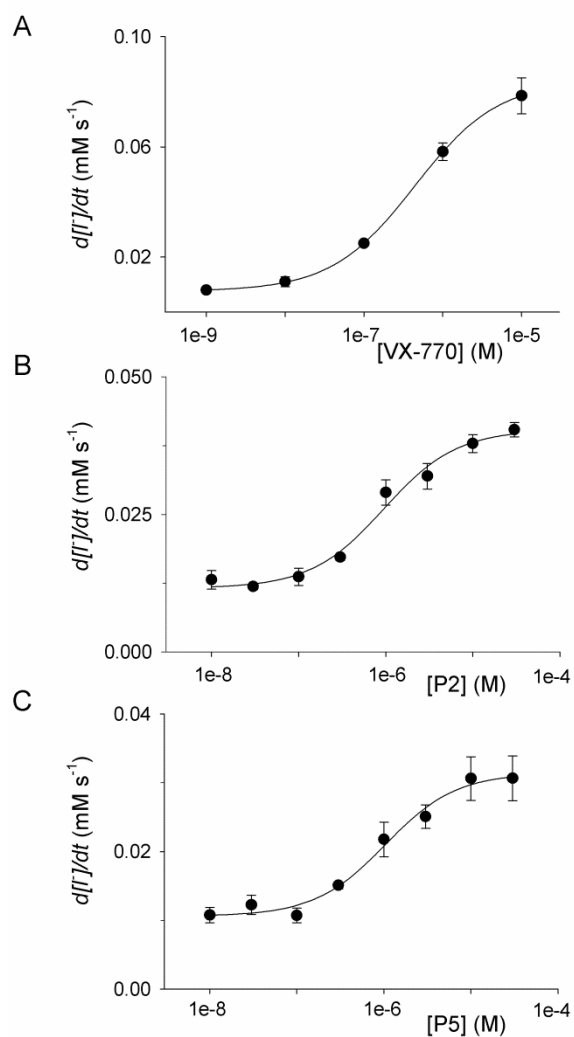
Figure 5. YFP-F508del-CFTR assay validation using known potentiators. All curves in the presence of 50 μM forskolin. A) VX-770, EC_{50} = 441 nM ± 144, n_H = 0.82 ± 0.2, n = 3 wells from 1 experiment. B) P2, EC_{50} = 0.95 μM ± 0.2, n_H = 1.04 ± 0.2, n = 5 or n = 6 wells from 2 experiments. C) P5, EC_{50} = 1.0 μM ± 0.4, n_H = 1.1 ± 0.4, n = 5 or n = 6 wells from 2 experiments. YFP-F508del-CFTR rescued using 30°C incubation for 24 h.
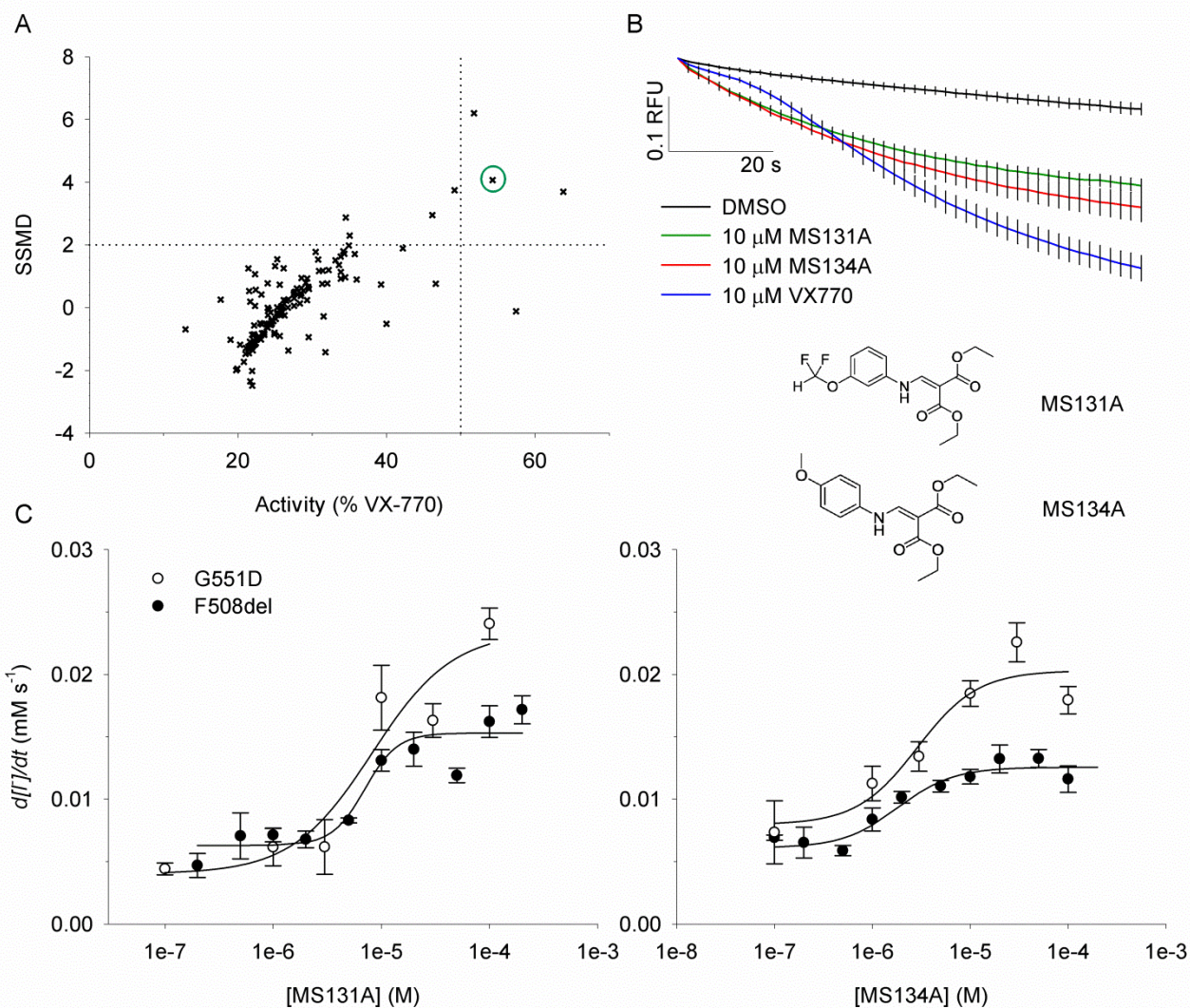
Figure 6. YFP-F508del-CFTR potentiator pilot screen results. A) Dual-flashlight plot. Each cross represents one test compound, tested 3 times. Compounds with SSMD value > 2 and activity > 50% compared to 10 μM VX-770 were selected as hits. B) Top: Quenching traces of hits identified in the pilot screen, alongside positive (10 μM VX-770) and negative (DMSO) controls. RFU: relative fluorescence units; traces shown from addition of activating compound. n = 3. Bottom: Structures of confirmed hit compounds. C) Concentration-response curves on F508del-CFTR and G551D-CFTR. MS131A EC_{50} = 7.0 μM ± 1.4 μM, n_H = 2.9 ± 1.4, and 8.2 μM ± 4.3 μM, n_H = 1.2 ± 0.6. MS134A EC_{50} = 1.8 μM ± 0.7 μM, n_H = 1.5 ± 0.7, and 2.9 μM ± 1.4 μM, n_H = 1.4 ± 0.8, on F508del-CFTR and G551D-CFTR, respectively. Potentiation was tested in the presence of 50 μM forskolin, and F508del-CFTR was rescued using temperature correction. n = 3 - 9 wells from 1 - 3 experiments.
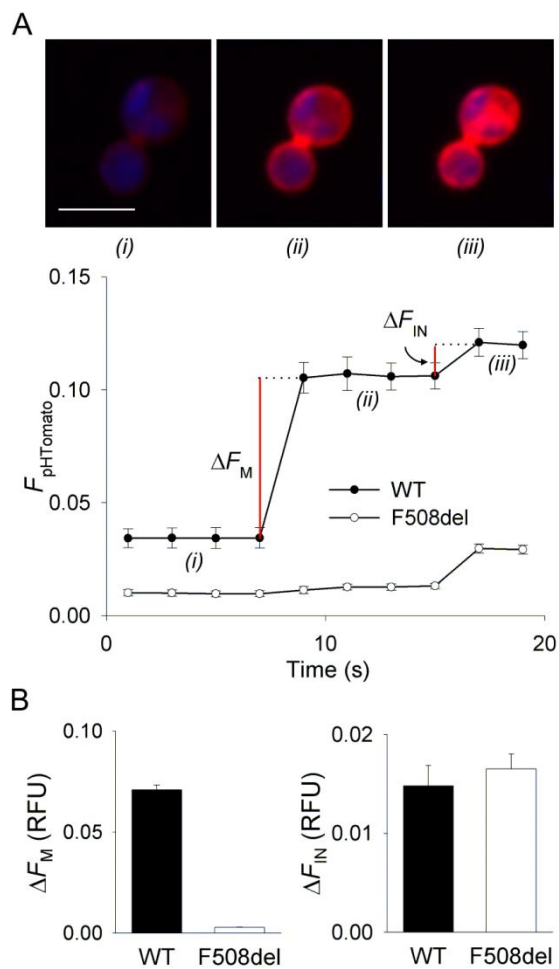
Figure 7. CFTR-pHTomato assay. A) Fluorescence images (WT) and traces (WT and F508del-CFTR) during the CFTR-pHTomato assay. *(i)* to *(iii)* refer to stages in the assay. Traces represent mean ± SEM of 3 wells in 1 experiment. Scale bar = 20 μm. B) Mean $\varDelta F_{M}$ and $\varDelta F_{IN}$ for WT-CFTR and F508del-CFTR, quantified from traces in A.
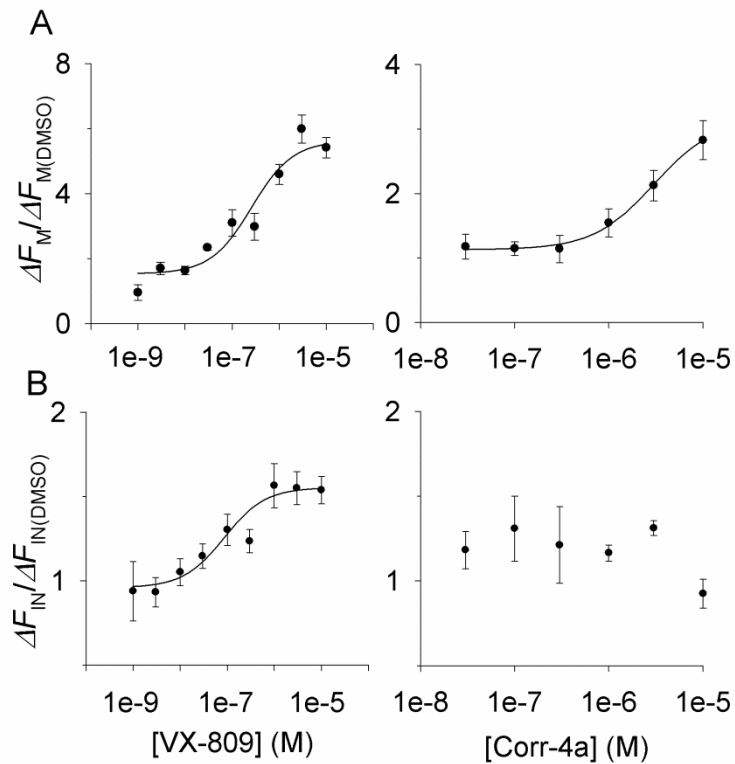
Figure 8. CFTR-pHTomato assay validation using known correctors. A) Membrane and B) Internal F508del-CFTR following 24 h incubation with VX-809 or Corr-4a, alongside temperature correction. VX-809 EC_{50} = 259 nM ± 97 nM and 87 ± 61 nM, for membrane and internal F508del-CFTR, respectively, n = 3 - 6 wells from 2 experiments. Corr-4a EC_{50} = 3 µM ± 2.3 µM, n_H = 1.35 ± 1, for membrane F508del-CFTR, n = 3 wells from 1 experiment. Correction expressed as fold increase compared to DMSO-treated controls.
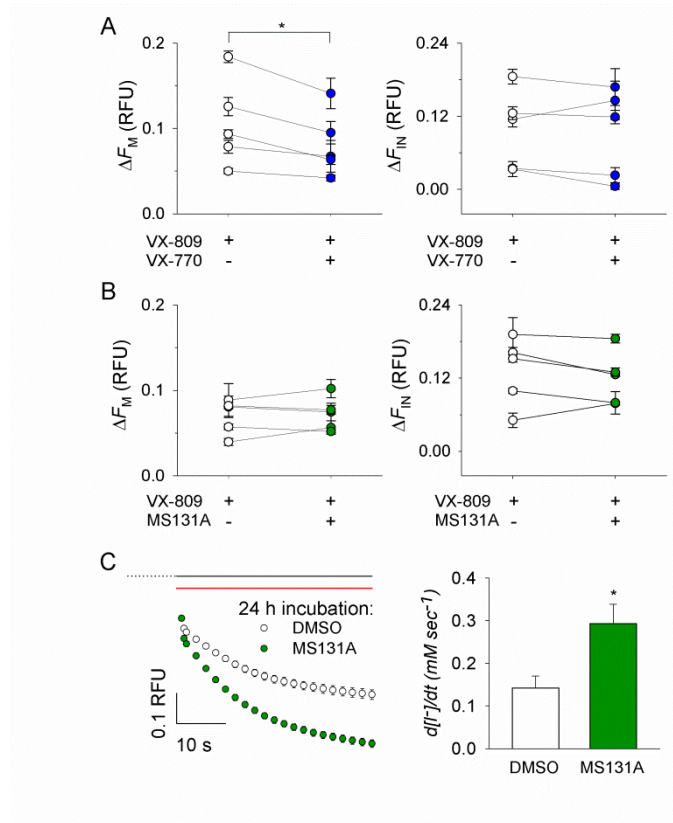
Figure 9. F508del-CFTR stability following 24 h incubation with VX-770 and MS131A. A) Membrane (left) and internal (right) F508del-CFTR following treatment with 10 μM VX-809 ± 10 μM VX-770. * p < 0.05 from paired t-test. B) Membrane and internal F508del-CFTR following 24 h incubation with 10 μM VX-809 ± 10 μM MS131A. Each symbol represents the mean (± SEM) of 3 wells from 1 experiment: lines connect different treatments from the same experiment. C) YFP-F508del-CFTR was corrected by low temperature incubation, in the presence or absence of 10 μM MS131A. 50 μM forskolin was pre-applied to the cells for 90 s (black dotted line) before Ⴈ addition (red line). YFP quenching is shown from Ⴈ addition. n = 9 from 3 experiments. * p < 0.05 from Mann-Whitney U test.